Noise thermometry applied to thermoelectric measurements in InAs nanowires

2016 Semicond. Sci. Technol. 31 104001

(http://iopscience.iop.org/0268-1242/31/10/104001)

IOP Publishing Semiconductor Science and Technology
Semicond. Sci. Technol. 31 (2016) 104001 (6pp) doi:10.1088/0268-1242/31/10/104001

Noise thermometry applied to thermoelectric measurements in InAs nanowires

E S Tikhonov[1], D V Shovkun[1], D Ercolani[2], F Rossella[2], M Rocci[2], L Sorba[2], S Roddaro[2] and V S Khrapai[3,4]

[1] Institute of Solid State Physics, Russian Academy of Sciences, 142432 Chernogolovka, Russian Federation
[2] NEST, Istituto Nanoscienze—CNR and Scuola Normale Superiore, Piazza S. Silvestro 12, I-56127 Pisa, Italy
[3] Moscow Institute of Physics and Technology, Dolgoprudny, 141700 Russian Federation

E-mail: dick@issp.ac.ru (V S Khrapai)

Received 13 February 2016, revised 3 June 2016
Accepted for publication 20 June 2016
Published 6 September 2016

Abstract

We apply noise thermometry to characterize charge and thermoelectric transport in single InAs nanowires (NWs) at a bath temperature of 4.2 K. Shot noise measurements identify elastic diffusive transport in our NWs with negligible electron–phonon interaction. This enables us to set up a measurement of the diffusion thermopower. Unlike previous approaches, we make use of a primary electronic noise thermometry to calibrate a thermal bias across the NW. In particular, this enables us to apply a contact heating scheme, which is much more efficient in creating the thermal bias as compared to conventional substrate heating. The measured thermoelectric Seebeck coefficient exhibits strong mesoscopic fluctuations in dependence on the back-gate voltage that is used to tune the NW carrier density. We analyze the transport and thermoelectric data in terms of an approximate Mott's thermopower relation and evaluate a gate-voltage to the Fermi energy conversion factor.

Keywords: noise, nanowire, thermoelectric, InAs

(Some figures may appear in colour only in the online journal)

Efficient thermoelectric (TE) conversion in solid state devices has been an elusive target for many decades. An ideal TE material should display a large electrical conductivity σ and Seebeck coefficient S, and a small heat conductivity κ [1]. On the other hand, bulk materials are typically characterized by a strong interdependence between these parameters, which poses limits to the maximum achievable conversion efficiency [1]. Nanostructured semiconductors currently offer a host of novel ways to elude part of these constraints and are leading to a promising new direction in TE research [2–4]. For instance, present evidence shows that phonon conductivity can be significantly suppressed in nanostructures [5–9] and promising results have also been obtained on the tuning of the TE response through engineering of electron quantum states [10–12]. The investigation of TE effects in nanoscale conductors, however, brings with it a set of technical challenges linked to reproducibility and accuracy in the estimate of the TE properties of single nanostructures. In particular, electrical and heat contact resistances [8, 9] are often difficult to predict and measure, as well as the relative impact of the different transport mechanisms in the emergence of the nanomaterials' TE properties. In addition, the role of phonons and their interaction with an electron system is often hard to access in a real nanostructure [13]. This calls for novel measurement methods to correlate various aspects of the TE response of a nanomaterial and sort out the fundamental physics ruling their TE behavior [14, 15].

In our work, we investigate the TE response of individual InAs NWs at a temperature of a few Kelvins and demonstrate a primary thermometry method based on current noise measurements. This technique, while being more complex than standard DC measurements, has a few advantages. First of all, this approach allows a direct measurement of the thermal bias across the device, and covers a fairly large operation

[3] Author to whom any correspondence should be addressed.

temperature range going well beyond that typically available with superconductive tunnel junctions [16]. In addition, we show that the investigation of shot noise as a function of the bias offers a valuable insight into the device transport regime. In particular, we identify that the electron–phonon energy exchange can be neglected for temperatures below ~40 K and transport is consistent with the elastic diffusion regime. This enables us to investigate the diffusion thermopower of the individual InAs NWs in the regime of strong mesoscopic fluctuations.

Device characterization

Au-assisted Se doped InAs NWs are grown by chemical beam epitaxy on an InAs(111) B substrate. The NWs of ≈70 nm diameter and 2 μm length were drop-casted on a doped silicon wafer with a 280 nm thick SiO_2 insulator on top. The carrier density of the InAs NWs derived by field effect measurements is about 1×10^{18} cm^{-3}. We performed the measurements in two ^{3}He inserts, with the samples immersed in gas (at $T = 4.2$ K). The noise spectral density was extracted from measurements of voltage fluctuations on the load resistor R_0 using home-made low-temperature amplifiers (LTamp) with a voltage gain of about 10 dB, input current noise of $\sim 10^{-27}$ A^2/Hz. The only active component of the amplifier is the Agilent HEMT ATF35143. We used a resonant tank circuit at the input of the LTamp, see the sketch in figure 1(a), with a ground bypass capacitance of a coaxial cable and contact pads ~40 pF, a hand-wound inductance of ~6 μH and a load resistance of 10 kΩ. The output of the LTamp was fed into the low noise room temperature amplification stage with a hand-made analogue filter and a power detector. The setup has a bandwidth of ~0.5 MHz around a center frequency of $f_0 \approx 10$ MHz. This resonant frequency is determined by the parasitic capacitance of the coaxial cable and of the sample at the input of the LTAmp. We checked that it is high enough to safely neglect the $1/f$ noise of the amplifier, which in our case is known to be insignificant at frequencies higher than 1 MHz. A calibration was achieved by means of equilibrium Johnson–Nyquist noise thermometry. For this purpose we used a commercial pHEMT transistor, connected in parallel with the device. Its resistance, and thus the contribution to the measured thermal noise signal, could be tuned via changing its gate voltage. Otherwise, the transistor was depleted and didn't influence the noise measurements. The result of such calibration is shown in the inset of figure 2, where we plot the measured thermal noise power as a function of the parallel resistance of the circuit, $R_{\|}^{-1} = R_{\rm NW}^{-1} + R_{\rm load}^{-1} + R_{\rm hemt}^{-1}$, at two different temperatures. Theoretical fit with the known bath temperature, L and f_0 allow us to determine the exact value of the amplifier's input current noise and are shown by the dashed lines in the figure (details of the data treatment can be found in the supplementary material associated with reference [17]). All transport measurements were performed with the help of a two-terminal or four-terminal lock-in resistance measurement.

In our experiments we used four devices of two different architectures shown in figure 1 and referred to as device I and device II. A larger scale SEM image of the device I is shown in figure 1(a) and the magnified inner part in figure 1(b). In the figures, the light gray color corresponds to the Ti/Au metallic layers evaporated on top of the SiO_2 substrate or a single InAs NW. Two contact stripes are used as ohmic contacts to the NW. Each stripe is shaped in the form of a four-terminal bar, whose narrower and thinner part is connected to the either end of the NW. One of them, marked N and greenish, is connected to the dc measurement setup and the low-temperature rf-amplifier via the terminal 1. This contact stripe serves for noise detection. The other one, marked H1 and yellowish, is used as a contact heater. In device I we also used a meander-shaped substrate heater, marked HS and blueish. Heating currents $I_{\rm H}$ serve to energize the heaters and create a thermal bias across the NW during the TE measurements. The remaining meander-shaped heater, as well as the plunger gates next to the NW, were not used and kept grounded in the present experiment. Figures 1(c) and (d) depict the layout of device II. This device is equipped with three contact stripes which divide the NW into a short and long section. The center contact, marked N, greenish, has the same meaning as for device I. The side contact stripes, marked H1 and H2, yellowish, are used as heaters for the short and the long sections, respectively. Device II lacks substrate heaters; its plunger gates were also not used in the present experiments. In the rest of the paper we discuss the results of the measurements obtained in the two representative samples of both architectures.

In figure 2 we characterize the transport regime in our NWs using the shot noise measurements at a bath temperature of $T_0 = 4.2$ K. Here we plot the noise spectral density S_I for device II in dependence of the NW bias current $I_{\rm NW}$, which flows via the terminal N to the grounded contact 1 or 3, via, respectively, the short or long NW section. In both cases, near the origin S_I crosses over from the equilibrium Johnson–Nyquist value $4k_{\rm B}T_0/R$ to a remarkably linear shot noise dependence $S_I = 2eFI_{\rm NW}$, that persists up to $|I_{\rm NW}| \approx 3$ μA in longer devices or even up to $|I_{\rm NW}| \approx 10$ μA in shorter devices and is characterized by a Fano factor $F \approx 0.3$, nearly the same for all the studied NWs. This linear behaviour in a wide range of currents demonstrates the absence of noise from resistance fluctuations, which is generally characterized by the parabolic dependence of S_I on the current. Such behavior is a hallmark of elastic diffusive transport, that is characterized by a universal value $F = 1/3$ [18, 19]. This value indicates the insignificance of e–e scattering [20] in our devices up to the carrier excess energies of at least 10 meV. Remarkably, this observation is far more favourable than the theoretical prediction which gives $\tau_{ee} \approx \tau_{\rm dwell}$ already at 2 meV [21]. Note, that minor deviations of F from $1/3$ in our experiment can be caused by mesoscopic shot noise fluctuations [22] and/or a calibration uncertainty. Such mesoscopic fluctuations are

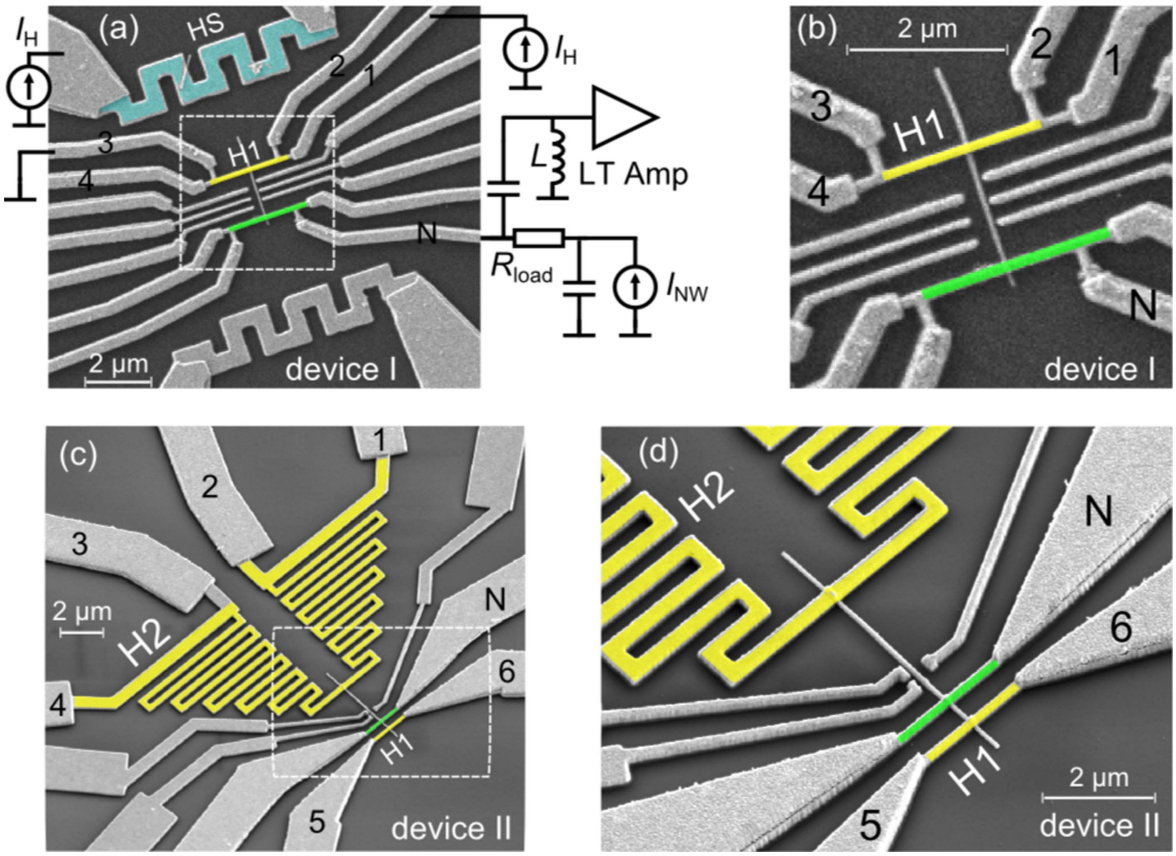

Figure 1. Scanning electron micrographs of two studied devices. (a, b) device I. (a) An InAs nanowire is connected to two identical 2 μm long Ti/Au metallic contact stripes which further form four-terminal bars. One of the stripes, marked as N and colored green, is used for the noise measurements, while the other one, marked as H1 and colored yellow, is used as a contact heater in the TE measurements. A few micrometers above the electrically isolated meander-shaped metallic substrate heater, marked as HS and colored blue, is located. The noise measurement scheme, attached to the terminal N, is given on the right hand side and is the same for both devices. In the TE measurements we set the heating current I_H through one of the heaters and measure the resulting voltage V_{th} between terminals N and 2. Terminal 3 was dc-grounded throughout all the experiments, while terminals 1, 2, 4 and 5 could be either grounded or left floating. All terminals are rf by-passed to ground by 10 nF capacitors. (b) Magnified inner part of the device. (c, d) device II. (c) An InAs nanowire is connected to three different contact stripes. Two stripes, marked as H1 and H2, colored yellow, are used as the contact heaters in the TE measurements, respectively, for the short and the long NW sections. The third in-between stripe N, colored green, is used for the noise measurements. In the TE measurements we set the heating current I_H through one of the heaters and measure the resulting voltage V_{th} between either terminals (5, 6) and N (for the short NW section) or terminals (2, 3) and N (for the long NW section). All terminals are rf by-passed to ground by 10 nF capacitors and can be either dc-grounded or left dc-floating during the experiment. (d) Magnified inner part of the device.

clearly visible as slight irregularities of the slope for the short section data, see the circles in figure 2. The elastic diffusive transport regime in our NWs was observed to break down only in longer devices for $|I_{NW}| \geqslant 3\ \mu A$, corresponding to a noise temperature above 40 K. Here, a gradual deflection of S_I from the linear dependence becomes evident at increasing $|I_{NW}|$, that results from the electron energy relaxation via acoustic phonon emission and can be used to estimate the inelastic *e–ph* scattering length [18]. Regarding TE experiments, this observation indicates that a mutual impact of non-equilibrium phononic and electronic NW subsystems, including possible electron–phonon drag effects, cannot be neglected for such high temperatures. Below we concentrate on a temperature range around $T_0 = 4.2$ K where such effects are not important and the TE experiment probes the diffusion thermopower.

Measurement of the NW thermal bias

It is convenient to treat diffusive transport and noise in our NWs within the quasi-classical approach [18] by means of local electronic energy distribution $f_{\varepsilon,x}$. For elastic diffusion the kinetic equation for $f_{\varepsilon,x}$ reduces to:

$$\frac{\partial^2 f_{\varepsilon,x}}{\partial x^2} = 0, \tag{1}$$

where x is a coordinate along the NW and ε is the electron energy relative to the Fermi level. The solution of the equation (1) is simply $f_{\varepsilon,x} = f_{\varepsilon,0}(1 - x/L) + f_{\varepsilon,L}(x/L)$, where $f_{\varepsilon,0}$ and $f_{\varepsilon,L}$ are the boundary conditions on the two ends of the NW. This solution also determines the spectral density of spontaneous current fluctuations in the NW via:

$$S_I = \frac{4}{R}\int \frac{\mathrm{d}x}{L}\int f_{\varepsilon,x}(1 - f_{\varepsilon,x})\mathrm{d}\varepsilon, \tag{2}$$

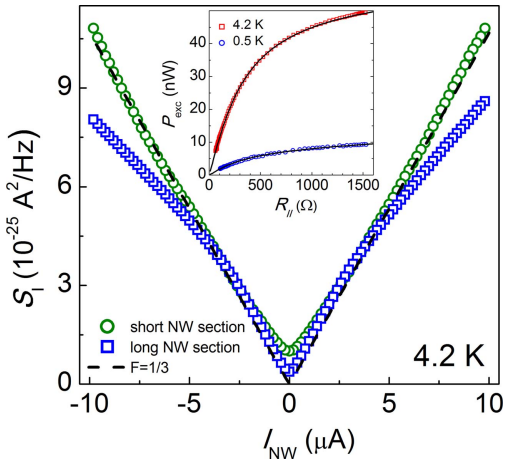

Figure 2. Characterization of the transport regime in our NWs. Shot noise spectral density as a function of current at $T = 4.2$ K for long (squares) and short (circles) sections of the NW device II. The slope of the dashed guide line corresponds to the Fano-factor $F = 1/3$. Inset: Johnson–Nyquist noise calibration. Variation of the measured thermal noise power (symbols) and the fits (solid lines), using known inductance L and the resonant frequency, as functions of $R_{||}$ (see text) for the two bath temperatures of $T = 4.2$ K and 0.5 K. Constant offset signal owing to the voltage noise of all the amplifiers is subtracted.

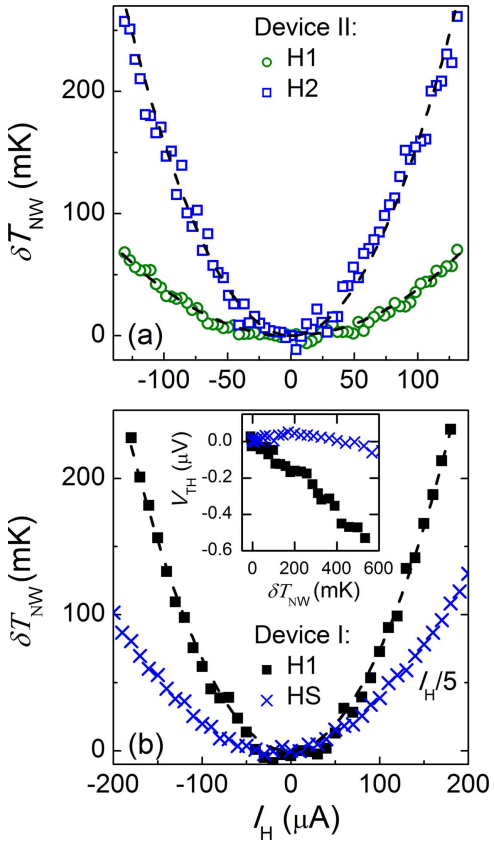

Figure 3. (a) Device II: Noise temperature change δT_{NW} of the short (circles) and long (squares) sections of the NW in response to the heating current I_H through the contact heaters H1 and H2, respectively. (b) Device I: Noise temperature change δT_{NW} of the NW in response to the heating current I_H through the contact stripe heater H1 (squares) and through the substrate heater HS (crosses), respectively. The dashed guide lines reflect the parabolic dependencies. Inset: comparison of induced TE voltages for contact (squares) and substrate (crosses) heaters for the same range of δT_{NW} values.

where R is the NW resistance. The equations (2) and (1) also define the NW noise temperature T_{NW} via a Johnson–Nyquist like relation $T_{NW} = \int T_N(x)\frac{dx}{L}$, where $T_N(x) = (k_B)^{-1}\int f_{\varepsilon,x}(1 - f_{\varepsilon,x})d\varepsilon$ is the noise temperature for a given position. For a uniform Fermi–Dirac distribution T_{NW} reduces to the usual equilibrium temperature. Below, we use the equations (1) and (2) to quantify the thermal bias across an individual NW.

In our TE experiments we mostly used a contact heating scheme, when the thermal bias δT across the NW is created by means of the heating current I_H, e.g. flowing between the terminals 1 and 3 via the contact heater H1 in figure 1(a). A similar approach was used in a thermoelectric experiment of [23]. A conceptual advantage of the present experiment, however, is that we use the noise thermometry to directly characterize the NW device under test, rather than to measure the average temperature of the metallic heater. The heating current modifies the energy distribution $f_{\varepsilon,0} = f_0 + \delta f_H$ at the hot-end of the NW ($x = 0$), whereas the opposite cold-end of the NW ($x = L$) remains in equilibrium $f_{\varepsilon,L} = f_0 \equiv (\exp(\varepsilon/k_B T_0) + 1)^{-1}$. While the leads of the NW are probably in the hot-electron regime at the highest currents applied, this may not be the case at low excitations. Thus, the modified distribution $f_{\varepsilon,0}$ is not necessarily thermal [24]. Therefore we define the thermal bias via the excess noise temperature on the hot-end $\delta T \equiv T_N(0) - T_0$. For small enough I_H a relation between δT and the noise temperature of the NW can be derived with the equations (1) and (2), namely:

$$\delta T_{NW} = \delta T/2, \tag{3}$$

where we introduced excess noise temperature of the NW $\delta T_{NW} = T_{NW} - T_0$. Note that this intuitive relation holds for elastic diffusive transport and an arbitrary energy distribution on the hot-end provided $\delta f_H \ll f_0$.

Equation (3) enables us to quantify the thermal bias across the NW by means of the noise thermometry [25]. In figure 3(a) we plot the measured δT_{NW} in dependence on I_H for the two sections of the NW device II. This experiment allows us to compare the heating efficiencies of the short and narrow contact heater H1 versus the long and wide contact heater H2 attached, respectively, to the short and long NW sections, see figure 1(b). For both the short section (circles) and the long section (squares) parabolic dependencies are observed as demonstrated by the dashed line fits of the form $\delta T \propto (I_H)^2$. This illustrates the fact that for small δT the temperature rise is proportional to the amount of the released Joule heat. Note, however, that in spite of a factor of ~10 difference between the two heater resistances the corresponding δT in figure 3(a) differs only by a factor of ~4. The reason is a smaller Joule heating efficiency of the long and wide heater H2 owing to the electron–phonon energy loss that is proportional to a heater volume and appears to be negligible for a short and narrow heater H1, see [25].

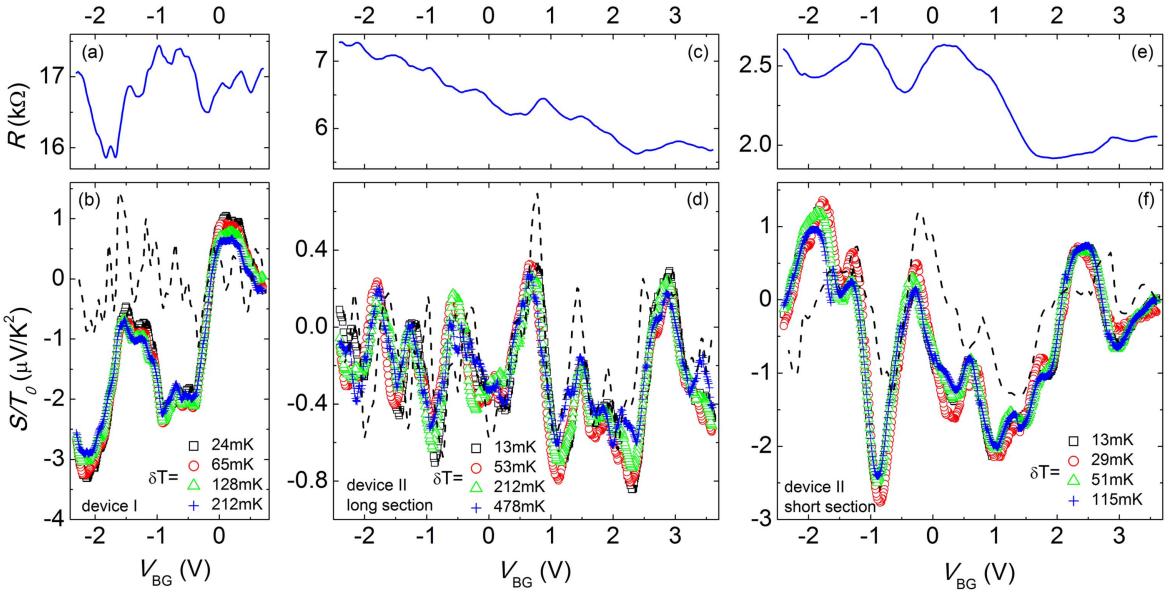

Figure 4. Linear response resistance and normalized Seebeck coefficient S/T_0 as a function of back-gate voltage measured on device I (a, b) and device II for short (c, d) and long (e, f) NW sections. Different symbols correspond to different values of the thermal bias, see respective legends. The dashed lines are numerically calculated from the data $R(V_{\rm BG})$ and the Mott's thermopower relation using a gate-voltage to the Fermi energy conversion factor $\alpha \sim 6.7$ meV/V, see text.

In figure 3(b) we compare the measured $\delta T_{\rm NW}$ for different heater types. Squares and crosses correspond, respectively, to the contact heater H1 and the substrate heater HS of the NW device I depicted in figure 1(a) (both heaters have about 3 Ω resistances). Again, the data follow a nearly parabolic functional dependence, as indicated by the dashed line for the contact heater. While the efficiency of the contact heater is comparable to the data of figure 3(a), the substrate heater is found to be much less efficient, so that we had to reduce the corresponding abscissa scale by a factor of 5. This emphasizes a relatively weak electron–phonon coupling in our devices, on which the substrate heating relies. In addition, we observe that unlike contact heating, substrate heating is less effective in creating a thermal bias across the NW. This is demonstrated by TE measurements in the inset of figure 3(b). Here, we plot the TE voltage $V_{\rm th}$ across the NW, which is identified as the voltage drop between the terminals N and 2 in device I symmetrized for positive and negative $I_{\rm H}$, see figure 1. We find that for the same $\delta T_{\rm NW}$, the $|V_{\rm th}|$ is much smaller when the substrate heater is used instead of the contact heater (crosses *vs* squares, respectively). Thus, the substrate heater tends to heat up the NW as a whole, which is not the case for the contact heating configuration. For this reason, in the following we concentrate on the TE measurements using the contact heaters.

Thermoelectric measurements

The applied thermal bias results in a TE voltage drop $V_{\rm th}$ between the heated end of the NW and the (equilibrium) contact N, which is kept open circuit during the TE measurement. We note that experimentally, $V_{\rm th}$ is a tiny contribution masked by a resistive voltage drop across the part of the current biased contact stripe heater and the corresponding incoming lead, which is involved in this measurement. For instance in device I, the resistive contribution comes from the lead, marked as 3, and the adjacent half of the heater stripe, see figure 1(a). In the following we modulate $I_{\rm H}$ with a small ac current 20–70 nA at a frequency of 11 Hz, that corresponds to δT in the range 10–500 mK, and measure the induced $V_{\rm th}$ using a lock-in second harmonic detection. We convert the data into the Seebeck coefficient $S \equiv V_{\rm th}/\delta T$, normalize it by the bath temperature and plot S/T_0. Figures 4(b), (d), (f) demonstrate, respectively, the data for device I, and for long and short NW sections of device II in dependence of the back-gate voltage $V_{\rm BG}$. In all three cases we observe the same qualitative behavior. Within a broad range of δT the datasets in each panel collapse on a single curve, justifying the linear dependence of $V_{\rm th}$ on δT. On average, the TE signal is apparently negative, on the order of $\overline{S}/T_0 \sim -1 \div -0.2\ \mu{\rm V/K^2}$, as expected for n-type charge carriers in our InAs NWs and consistent with previous studies [14]. Yet, the overall TE signal is dominated by pronounced mesoscopic fluctuations that even cause a sign reversal of S in certain gate-voltage ranges. Although the peak value of the Seebeck coefficient may be increased due to this mesoscopic effect, in applications such uncontrolled fluctuations are hardly to be exploited since in a real device, consisting of the whole array of nanowires, they would average out. The mesoscopic origin of the fluctuations is consistent with the two following observations. First, the strongest fluctuations are found in the most resistive device I. Second, the fluctuations are weaker in the longer section of device II, consistently with the length dependent self-averaging. Note also, that our NWs are highly doped and characterized by a relatively small resistance and diffusive transport mechanism, as verified via shot noise, see figure 2. This is in contrast to the

lower doping NWs for which the fluctuations of S were interpreted in terms of quantum dot-like states [12].

Below we compare the TE measurements with the behavior of the gate-voltage dependent resistance R. As shown in figures 4(a), (c) and (e) for the respective measurement configurations, the measured R exhibits small random fluctuations as a function of V_{BG}, that tunes the carrier density and the chemical potential of the NW electron system. According to Mott's thermopower law [26] the energy dependence of the conductivity and the TE response are related as $S/T_0 = -(\pi k_B)^2/(3e\sigma)\mathrm{d}\sigma/\mathrm{d}E_F$, where the derivative is evaluated at the Fermi energy. Assuming a linear dependence of E_F on V_{BG}, in figures 4(b), (d) and f we plot the numerically calculated Mott's law $(\pi k_B)^2/(3eR\alpha)$ $\mathrm{d}R/\mathrm{d}V_{BG}$ (dashed lines), where $\alpha = \mathrm{d}E_F/\mathrm{d}V_{BG}$. The results differ for the two devices. For device II, both short and long sections, the fluctuations of S are correlated with the Mott's law data, see figures 4(d) and (f). This similarity enables us to evaluate a gate-voltage to the Fermi energy conversion factor at $\alpha \sim 7$ meV/V. This value of α is consistent with estimates of the density of states and the back gate capacitance in our NWs, as well as with the assumption of slow variation of $\sigma(E)$ on the scale of $k_B T_0$, which is implied by Mott's law. By contrast, no obvious correlation between the measured and evaluated S is observed for device I (figure 4(b)). Moreover, the typical V_{BG} scale of the resistance fluctuations is considerably shorter than the one for the TE signal. Most probably, this is a consequence of a much stronger impact of charge carrier traps on the gate-voltage swept resistance data in this sample, which caused hysteresis and was the reason for the narrower sweep range in device I.

Summary

In summary, we applied a primary noise thermometry to investigate charge and TE transport in individual InAs NWs. This served to identify an elastic diffusive transport regime in our devices with negligible electron–phonon interaction at low temperatures. In TE measurements, the noise thermometry enabled us to use a contact heating approach, that turned out to be much more efficient than conventional substrate heating in creating a thermal bias across the NWs. With this approach, we measured the Seebeck coefficient S in two devices at $T_0 = 4.2$ K in dependence on the back-gate voltage. We observed pronounced random mesoscopic fluctuations of S, identified their rough correlation with the mesoscopic resistance fluctuations via the Mott's thermopower law in one device and evaluated a gate-voltage to the Fermi energy conversion factor. Our results demonstrate primary noise thermometry as a powerful tool for mesoscopic thermal transport applications, which is perfectly compatible with standard measurement techniques.

Acknowledgments

This work was supported in part by the Russian Academy of Sciences, the CNR through the bilateral CNR-RFBR projects 2015–2017, the Ministry of Education and Science of the Russian Federation Grant No.14Y.26.31.0007, the RFBR Grants 15-02-04285 and 15-52-78023. FR and MR acknowledge the support by the MIUR through the programs \FIRB - Futuro in Ricerca 2013 'Project \UltraNano' (Grant No. RBFR13NEA4).

References

[1] Snyder G J and Toberer E S 2008 *Nat. Mater.* **7** 105
[2] Majumdar A 2004 *Science* **303** 777
[3] Dresselhaus M S, Chen G, Tang M Y, Yang R G, Lee H, Wang D Z, Ren Z F, Fleurial J-P and Gogna P 2007 *Adv. Mater.* **19** 1043
[4] Shi L 2012 *Nanoscale and Microscale Thermophysical Engineering* **16** 79
[5] Boukai A I, Bunimovich Y, Tahir-Kheli J, Yu J-K, W A G III and Heath J R 2008 *Nature* **451** 168
[6] Hochbaum A I, Chen R, Delgado R D, Liang W, Garnett E C, Najarian M, Majumdar A and Yang P 2008 *Nature* **451** 163
[7] Martinez J A, Provencio P P, Picraux S T, Sullivan J P and Swartzentruber B S 2011 *J. Appl. Phys.* **110** 074317
[8] Swinkels M Y, van Delft M R, Oliveira D S, Cavalli A, Zardo I, van der Heijden R W and Bakkers E P A M 2015 *Nanotechnology* **26** 385401
[9] Zhou F *et al* 2011 *Phys. Rev.* B **83** 205416
[10] Heremans J P, Jovovic V, Toberer E S, Saramat A, Kurosaki K, Charoenphakdee A, Yamanaka S and Snyder G J 2008 *Science* **321** 554
[11] Tian Y, Sakr M R, Kinder J M, Liang D, MacDonald M J, Qiu R L J, Gao H-J and Gao X P A 2012 *Nano Lett.* **12** 6492
[12] Wu P M, Gooth J, Zianni X, Svensson S F, Gluschke J G, Dick K A, Thelander C, Nielsch K and Linke H 2013 *Nano Lett.* **13** 4080
[13] Hoffmann E A, Nilsson H A, Matthews J E, Nakpathomkun N, Persson A I, Samuelson L and Linke H 2009 *Nano Lett.* **9** 779
[14] Roddaro S, Ercolani D, Safeen M A, Suomalainen S, Rossella F, Giazotto F, Sorba L and Beltram F 2013 *Nano Lett.* **13** 3638
[15] Yazji S, Hoffman E A, Ercolani D, Rossella F, Pitanti A, Cavalli A, Roddaro S, Abstreiter G, Sorba L and Zardo I 2015 *Nano Res.* **8** 4048
[16] Giazotto F, Heikkilä T T, Luukanen A, Savin A M and Pekola J P 2006 *Rev. Mod. Phys.* **78** 217
[17] Tikhonov E S, Melnikov M Y, Shovkun D V, Sorba L, Biasiol G and Khrapai V S 2014 *Phys. Rev.* B **90** 161405
[18] Nagaev K E 1992 *Phys. Lett.* A **169** 103
[19] Beenakker C W J and Büttiker M 1992 *Phys. Rev.* B **46** 1889
[20] Steinbach A H, Martinis J M and Devoret M H 1996 *Phys. Rev. Lett.* **76** 3806
[21] Quinn J J and Ferrell R A 1958 *Phys. Rev.* **112** 812
[22] de Jong M J M and Beenakker C W J 1992 *Phys. Rev.* B **46** 13400
[23] Strunk C, Henny M, Schönenberger C, Neuttiens G and Van Haesendonck C 1998 *Phys. Rev. Lett.* **81** 2982
[24] Pothier H, Guéron S, Birge N O, Esteve D and Devoret M H 1997 *Phys. Rev. Lett.* **79** 3490
[25] Tikhonov E S, Shovkun D V, Ercolani D, Rossella F, Rocci M, Sorba L, Roddaro S and Khrapai V S 2016 Local noise in a diffusive conductor *Sci. Rep.* **6** 30621
[26] Mott N F and Jones H 1958 *The Theory of the Properties of Metals and Alloys* (New York: Dover Publications)